Meta-KANSEI modeling with Valence-Arousal fMRI dataset of brain

Article

Accepted Version

Shi, F., Dey, N., Ashour, A. S., Sifaki-Pistolla, D. and Sherratt, R. S. (2019) Meta-KANSEI modeling with Valence-Arousal fMRI dataset of brain. Cognitive Computation, 11 (2). pp. 227-240. ISSN 1866-9964 doi: https://doi.org/10.1007/s12559-018-9614-5 Available at https://centaur.reading.ac.uk/80563/

Meta-KANSEI modeling with Valence-Arousal fMRI dataset of brain

Fuqian Shi[a, *], Nilanjan Dey[b], Amira S. Ashour[c], Dimitra Sifaki-Pistolla[d], and R. Simon Sherratt[e]

a. College of Information and Engineering, Wenzhou Medical University, Wenzhou, 325035, PR China
b. Dept. of IT, Techno India College of Technology, West Bengal, 740000, India
c. Department of Electronics and Electrical Communications Engineering, Faculty of Engineering, Tanta University, Tanta, 31111, Egypt
d. School of Medicine, University of Crete, Heraklion, 71003, Greece
e. Department of Biomedical Engineering, the University of Reading, RG6 6AY, UK

* Corresponding author: Fuqian Shi, email: sfq@wmu.edu.cn, Tel.: +86-577-86689913, Fax: +86-577-86699222

Conflict of Interest:
Fuqian Shi declares that he has no conflict of interest. Nilanjan Dey declares that he has no conflict of interest. Amira S. Ashour declares that she has no conflict of interest. Dimitra Sifaki-Pistolla declares that she has no conflict of interest. R. Simon Sherratt declares that he has no conflict of interest.

Abstract

Background: Traditional KANSEI methodology is an important tool in the field of psychology to comprehend the concepts and meanings; it mainly focusses on semantic differential methods. Valence-Arousal is regarded as a reflection of the KANSEI adjectives, which is the core concept in the theory of effective dimensions for brain recognition. From previous studies, it has been found that brain fMRI datasets can contain significant information related to Valence and Arousal. **Methods:** In this current work, a Valence-Arousal based meta-KANSEI modeling method is proposed to improve the traditional KANSEI presentation. Functional Magnetic Resonance Imaging (fMRI) was used to acquire the response dataset of Valence-Arousal of the brain in the amygdala and orbital frontal cortex respectively. In order to validate the feasibility of the proposed modeling method, the dataset was processed under dimension reduction by using Kernel Density Estimation (KDE) based segmentation and Mean Shift (MS) clustering. Furthermore, Affective Norm English Words (ANEW) by IAPS (International Affective Picture System) were used for comparison and analysis. The data sets from fMRI and ANEW under four KANSEI adjectives of angry, happy, sad and pleasant were processed by the Fuzzy C-Means (FCM) algorithm. Finally, a defined distance based on similarity computing was adopted for these two data sets. **Results:** The results illustrate that the proposed model is feasible and has better stability per the normal distribution plotting of the distance. The effectiveness of the experimental methods proposed in the current work was higher than in the literature. **Conclusions:** mean shift can be used to cluster and central points based meta-KANSEI model combining with the advantages of a variety of existing intelligent processing methods are expected to shift the KANSEI Engineering (KE) research into the medical imaging field.

Keywords:

meta-KANSEI modeling; Valence-Arousal; kernel density estimation segmentation; mean shift clustering; fuzzy c-means; Affective Norm English Words

1. Introduction

Emotional psychology studies, including the emotional expression, emotional signal acquisition and processing, and emotional understanding attract the researchers' interest. In fact, it is an interdisciplinary research, involving cognitive science, biomedicine, information science and other fields. Harmonious natural human-computer interaction [1-3] and emotional computing technology [4] research is inseparable from emotional psychological theory and methods. Amongst the methods of emotional representation, the classical method aims to cluster the emotional vocabulary and obtain a qualitative representation of the emotion category. Based on the expression of emotional dimension, psychologists have considered emotional dimension labeling on Natural Language (NL). For example, the ANEW (English Vocabulary Emotional Library) of the National Institute of Mental Health (NIMH), have manually calibrated the emotional dimensions of more than 1,000 commonly used English words. Bradley and Cuthbert's image emotion library (IAPS), sound emotional library (IADS), and the text emotional library (ANET), were all obtained by manual calibration. The basic method of manual calibration is to give dimension to the values of words, pictures, sounds or texts directly by many people, and then estimate the statistical average of the dimension of each word, picture, sound or text [5-8]. This has an important practical significance for the tracking of the social dynamics reflected by the network emotion. It also illustrated the dimensionality emotion data acquired by the ANEW database, which is the cornerstone of emotional computing and high-level semantic modeling.

KANSEI Engineering (KE) is an innovative engineering branch that has a wide range of applications in automotive, toys, and in product shape design [9-13]. Recently, psychology and brain science research shifted the traditional KE research into new directions and brain KE was addressed subsequently. The mapping between the product visual observation and the expression of the human sensibility cannot be accurately established. However, this can be achieved under some weakened conditions. Human physiological body signals can be used to further develop KE. Following this development, brain imaging technology, such as an electroencephalograph (EEG) allows researchers to measure and obtain individual physiological signals [14] [15], thus emphasizing the KANSEI semantic recognition technology development. Furthermore, functional magnetic resonance imaging (fMRI) has been used to measure individual dimensions of sensitivities in neuroscience and psychology, being a noninvasive, space-time, high-resolution brain imaging technique. Using fMRI technology to study conceptual formation will assist the depth expression mechanism of KANSEI semantics. In addition, obtaining corresponding basic datasets of the KANSEI dimension along with brain imaging leads to further research perspectives on the cross fusion of KE and brain cognitive science. By using the new methods, including statistical learning, meta-clustering, and local preserving learning, brain imaging data can be used not only for pretreatment of brain conditions, but also for KANSEI conceptual modeling, such as KANSEI boundary calculation, and KANSEI similarity calculation. The development of new and effective mathematical tools will greatly reduce the expression gaps between

high-level semantic and low-level physiological signal. Externally calibrated psychometric quantities can guide the product design and engineering practice, but this coarse-grained, linear external calibration method has a large subjective bias [16]. Many medical experiments have shown the specific chemosensory domain of the two brains of the mygdala and the orbital frontal cortex and the pleasure of human emotion - positive or negative [17-19]. Kensinger and Corkin [20], and Kensinger and Schacter [21] also confirmed that the use of the different emotional vocabulary of short stimulation (about 2 seconds) from magnetic resonance imaging data analysis to the amygdala and orbital frontal cortex, two parts of the signal were significantly enhanced. However, different emotional vocabulary and different degrees of stimulation can determine the signal characteristics corresponding to those two brain chemical receptors. Lewis *et al.* [22] observed the effect of different emotional words (affective words) and different levels of stimulus on specific brain areas, including orbital frontal cortex, anterior cingulate gyrus, brain Island, amygdala, brain stem, pontine and striatum and other parts of the active peak, indicating that Valence – Arousal has a high degree of correlation with these parts. Furthermore, it can be determined that the orbital frontal cortex and amygdala are highly related to Valence and Arousal respectively. The multi-voxel pattern analysis method (MVPA) working on semantic features of brain signals was identified in different feature spaces of the brain signals [23].

Janata *et al*. [24] conducted a brain fMRI study of auditory and emotional information by tracking the activation characteristics of the Rostromedial area neurons in the prefrontal cortex. It was found that neurons in this region showed selective activation of different emotional intensities, where the activation state of the sensory neurons was maintained in the cortex as a dynamic topological map. In fact, other fMRI studies of stimulating emotional information have shown the presence of specific chemical receptors in the human brain, such as the amygdala and the orbital frontal cortex responses is necessarily linked [25-27]. In addition, other brain imaging methods also play an active role. Sardouie *et al*. [28] used EEG for Time-Frequency Priors. Frantzidis *et al*. [29] revealed a relationship between neuro-physiological signals and emotional states from the EEG using wavelet transform and a Support Vector Machine (SVM). Similarly, Murugappan *et al*. [30] employed the wavelet transform method along with fuzzy clustering analysis of the EEG data to several typical significances of the evaluation index. Using brain imaging techniques, researchers have demonstrated that affective stimuli have multiple effects on human brain activity. Of note, Hui and Sherratt [31] also used IAPS to create a wearable device for emotion recognition from physiological signals being the physical manifestation of emotional states. Thus it was proven that the study of cognitive mechanisms of brain cognition have important applications in medical treatment. These works built up the relationship between the low-level physiological emotion signals and the high-level semantic concepts, but also provide a scientific basis to the study of emotional word modeling in the current work.

Based on this trend and demand, the current work established a meta-KANSEI calculation model based on the Valence-Arousal dimensional brain imaging data sets. A de-noising and dimension reduction method has been developed for brain imaging on a data volume, and a meta-KANSEI presentation method has been conducted subsequently. Since product KANSEI mining plays a key role in the initial “idea generation” stages of the industrial design, more accurate formal model of dimensional expression of KANSEI semantics that can be further applied in intelligent design, intelligent interactive design, and the automatic reasoning system. Consequently, a meta-KANSEI computing model with high interpretability has been utilized in the present work for further revealing

the formation mechanism of product-consumer interaction evaluation.

In addition, Kernel Density Estimation (KDE) based image segmenting has been employed. KDE is typically used in probability theory to estimate the unknown density function. KDE has been widely used in many fields, for example, Haben and Giasemidis [32] combined the kernel density estimation and quintile regression techniques for probabilistic forecasts. Miao *et al*. [33] created a new analytical approach designated as the mixture kernel density model highly accurate estimation of wind speed probability distributions. Yuan *et al*. [34] developed an efficient unsupervised feature learning approach with density information and the proposed method was evaluated on the assembled congested scene dataset. Rodrigues *et al.* [35] created a hierarchically structured prior, defined over a set of univariate density functions using convenient transformations of Gaussian processes. The proposed KDE framework with segmentation and mean-shift clustering based meta-KANSEI modeling for brain Valence-Arousal fMRI dataset is illustrated in Fig. 1.

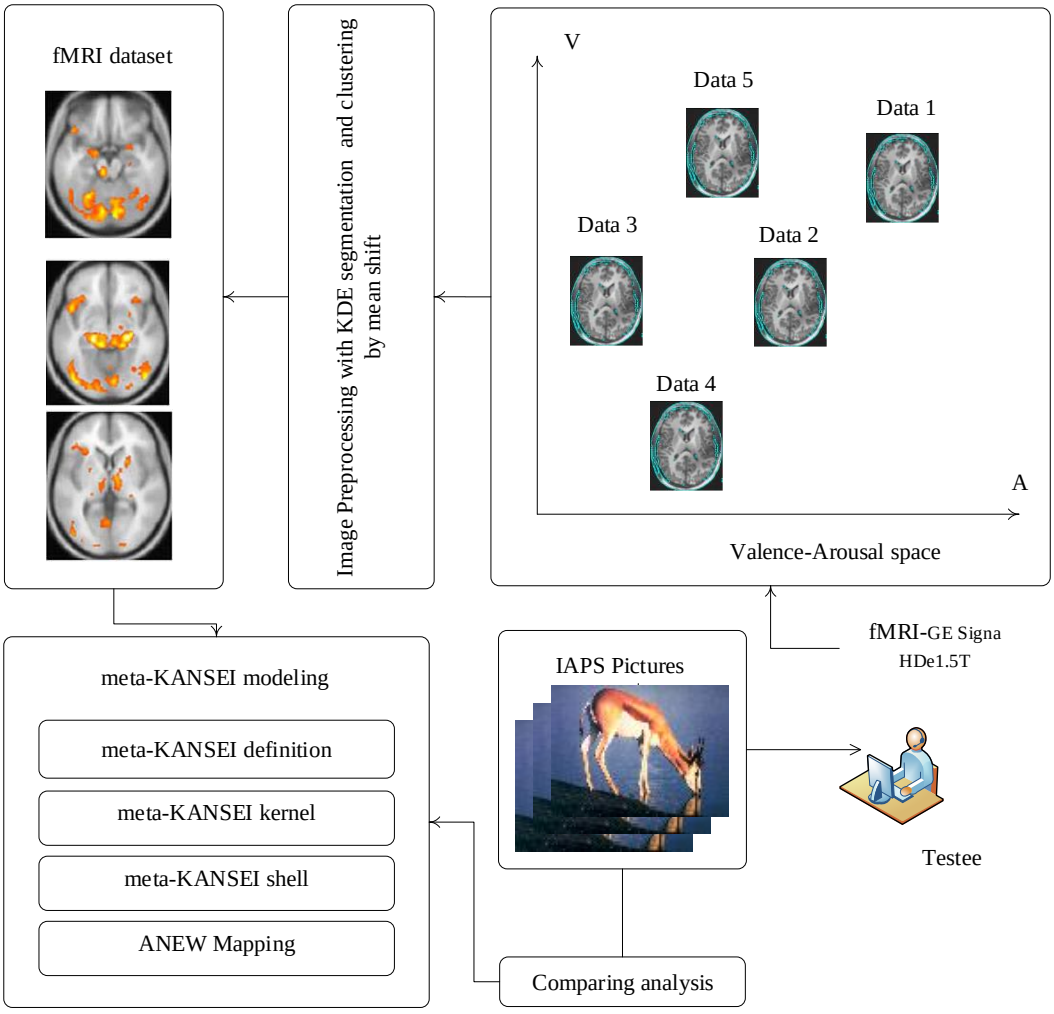

Figure 1. The frameworks of meta-KANSEI modeling employing mean-shift clustering and kernel density estimation segmenting of brain Valence-Arousal fMRI dataset

As illustrated in Fig. 1, after segmentation, the proposed approach in the current work learns the central sets of the meta-KANSEI model. *k*-means clustering was widely used because of its simplicity.

However, there are some problems, such as over-reliance on sample banks, prior knowledge, and lack of stability. Furthermore, fuzzy c-means (FCM) was used as an improvement to *k*-means to solve practical problems. In the current work, the mean shift-based clustering was developed and improved for fMRI dataset clustering [36].

The mean shift algorithm is an effective statistical iterative algorithm which is a randomly selected region with center "o" and radius "h" in the sample and obtain the average of all the sample points in the region. The sample density at the center must be smaller or equal than the sample density at the mean. Afterwards, the same steps are repeated with the mean value as the new center until converging to the maximum density. The mean shift is an algorithmic process, which is simple and easy to understand, so the iterative efficiency is very high. However, to ensure more accurate and efficient algorithm, while also depending on the iterative bandwidth at the middle of the set, the bandwidth of the iterative results for different results have a very important impact. Recently, many methods have been proposed to solve this problem, but these methods make the calculation more complicated and the iterative efficiency is reduced [37]. Therefore, it is necessary to improve the kernel function bandwidth selection for the applied algorithm to the practical problems. The mean shift method is widely used in images clustering. Ghassabeh [38] introduced the mean shift algorithm with Gaussian kernel. Ibrahim *et al*. [39] proposed the Interdependence Adaptive Scale Mean Shift (IASMS) algorithm for eye tracking. Duong *et al*. [40] developed a nearest neighbor estimator of the order derivatives of the probability density function using mean shift clustering. Consequently, Chen *et al*. [41] improved a Mean Shift Tracking (MST) algorithm and an Expectation-Maximization (EM)-like (IEML) for the query Region of Interest (ROI) of image. For fMRI dataset processing, Ai *et al*. [42] examined the temporal characteristics of acquired fMRI data with Mean-Shift Clustering (MSC) for fMRI analysis to enhance activation detections. Ghassabeh and Rudzicz [43] investigated the connection between the asymptotic bias of the well-known Nadaraya-Watson kernel regression and the Mean Shift (MS) vector with the Gaussian kernel.

2. Methods

2.1 Meta-KANSEI mapping of fMRI data

The obtained evaluation of the KANSEI state description corresponds to discrete points in emotional space. The Valence-Arousal space provides the basis for the quantitative representation of KANSEI semantics. However, people are more accustomed with emotional words to express emotional state. Coarse-grained emotional words have easy to understand features. Therefore, it is necessary to combine high-level semantic interpretation of KANSEI information with ANEW, which is a kind of emotional lexicon system of the National Institute of Mental Health (NIMH) to obtain fine-grained KANSEI semantic representation.

The emotion recognition based on brain imaging was applied after the coarsening of KANSEI semantics. The brain imaging data was correlated with sensory vocabulary. Typically, the KANSEI semantic recognition based on brain imaging is considered as the main problem to establish the KANSEI semantic computing model. The brain imaging mode corresponding to the different sensory vocabulary was examined by clustering. Furthermore, the main pattern recognition methods, such as the Artificial Neural Network (ANN), SVM or Fuzzy Inference System (FIS), can solve the

effectiveness of the recognition problem, especially to reduce the dimensionality of the brain imaging data to compare the effectiveness of the method. The main contribution of the current work is to validate the meta-KANSEI modeling method under the mapping with meta-KANSEI and fMRI dataset as show in Fig. 2.

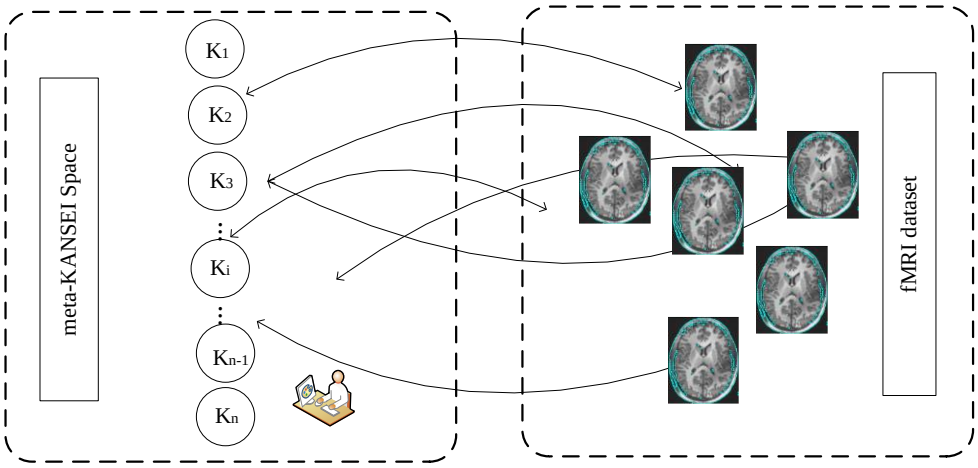

Figure 2. Mapping between of meta-KANSEI and fMRI dataset

The mapping relation can be the basic research for meta-KANSEI modeling, in fact, the mapping relation is based on the features of fMRI dataset and a certain KANSEI adjective such as $K_1, K_2, ...K_n$.

2.2 Meta-KANSEI modeling

2.2.1 The model presentation

The meta-sensible semantic representation can be divided into hyper-plane, super (ellipsoidal) and mixed type by a central topological type. This section first constructs a new multi-dimensional sensory information representation and processing system. The KANSEI semantics in a multi-dimensional eigen-space is essentially an abstraction, which is a multi-dimensional dataset with spatial topological structure and uncertainty measure. This can be formalized as a four-tuple $<U, P, d, \rho>$, where U is the universe of discourse, P is a node set with topological structure representing a typical set of entities, d is a distance measure defined on U, ρ is a Probability Density Function (PDF) defined on the measure space, which reflects the concept of concentration. This representation is particularly suitable for the organization and expression of multi-dimensional KANSEI semantics as well as the semantic reasoning of indeterminate information. In addition, this topic will study the KANSEI semantic information corresponding to the KANSEI body topology. In terms of topological structure, the information bodies of meta-nonsensibility have multi-dimensional nodes, hyper-planes, hyper-sphere or hyper-ellipsoid structures. Any KANSEI information semantic feature can be sufficiently close to the probability of the KANSEI body or can be described by a probability

distribution defined in the distance space, which essentially measures the uncertainty of the meta-sensory body boundary, and its granularity which is represented by the topological structure of the KANSEI body and the concept density distribution function.

2.2.1.1 Definitions on kernel of meta-KANSEI

Definition 1: suppose that universe is Ω , P is a KANSEI evaluation, $\forall P \in \Omega$, $\Omega = \{(E_1, E_2, ..., E_n) : E_i \in P$, E_i is the i -th dimensional of P . Hence, in Valence-Arousal space, let $P = (Valence, Arousal)$, which can be simplified as:

$$P = (v, a), \Omega = \{(v, a) \mid v, a \in R\} \tag{1}$$

where v , a are the Valence and Arousal values of a given KANSEI adjective respectively.

Definition 2: given a metric $d = \|\cdot\|$ in Valence-Arousal space satisfying:

$$d(P) = \|P\| = \sqrt{(v^2 + a^2 + d^2)} \tag{2}$$

$$d(P \pm Q) = \|P \pm Q\| = \sqrt{((v_P \pm v_Q)^2 + (a_P \pm a_Q)^2 + (d_P \pm d_Q)^2)}, \forall P, Q \in \Omega \tag{3}$$

$\forall \alpha, \beta \in R, P, Q \in \Omega$, where:

$$d(\alpha P \pm \beta Q) = \|\alpha P \pm \beta Q\| = \sqrt{(\alpha v_P \pm \beta v_Q)^2 + (\alpha a_P \pm \beta a_Q)^2 + (\alpha d_P \pm \beta d_Q)^2} \tag{4}$$

Obviously, from (4):

$$d(\alpha P + \beta Q) \leq |\alpha| \cdot d(P) + |\beta| \cdot |d(Q) \tag{5}$$

Definition 3: for point set $\{P_k^l \mid l = 1, 2, \cdots\}$, the kernel point is defined as:

$$P_k = \sum_l P_k^l = [\sum_l P_{k1}^l, \sum_l P_{k2}^l, \cdots \sum_l P_{kn}^l] \tag{6}$$

where P_{ki}^l presents the l^{th} point of the k^{th} meta-KANSEI's i^{th} dimension.

Definition 4: $\forall P_k \in \Omega$, there has a P_k centered neighborhood $N_{P_k}^{\varepsilon}$:

$$N_{P_k}^{\varepsilon} = \{X \mid \|P_k - X\| < \varepsilon, X \in \Omega\} \tag{7}$$

Definition 5: Upper Approximation Boundary:

$$UP_B = \{P_l \mid P_l \in N_{P_K}^u\} \tag{8}$$

Definition 6: Lower Approximation Boundary:

$$LP_B = \{P_l \mid P_l \in N^t_{P_K}\} \tag{9}$$

The boundary is $P_B = UP_B \setminus LP_B = B(u,t)$, and $P_B = P_K + \lambda(P_B - P_K)$, $\lambda \in [0,1]$ as shown in Fig. 3.

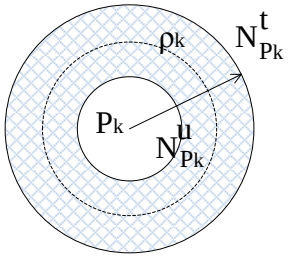

Figure 3. The structure of meta-KANSEI model

Normally, there are three types of kernels in the model, being single, flat and sphere. In the present research, we used the sphere kernel for calculation due to its symmetrical characteristic, so that we can calculate all directions using the same algorithm.

Definition 4: single point kernel

For KANSEI K, if the distribution of a given KANSEI adjectives in Valence-Arousal is a single point, so the kernel of the meta-KANSEI can be defined as:

$$\{P_K\}, P_K = \frac{1}{\|K\|}\sum_{P_i \in K} P_i(\rho(P_i)) \tag{10}$$

where $\rho(P_i)$ is the density of P_i.

Definition 5: Sphere kernel:

$$\{P_j \mid P_j \in N^{\varepsilon}_{P_K}\} \tag{11}$$

where $P_K = \frac{1}{\|K'\|}\sum_{P_i \in K'} P_i(\rho(Pi)), K' \subset K$ and $K' = \{P_i \mid \rho(P_j) \le \rho_T\}$. ρ_T is a constant used to limit the size of the kernel. Essentially, the kernel is a sphere with radius ε and the center of the sphere P_K is considered the center of gravity (the center of gravity in the sense of probability density) of a sphere whose density is greater than a given value which is a threshold for controlling the population of the model.

Definition 6: The planet set kernel is defined as the union of multiple sphere kernels as $\{\bigcup_i P_K\}$, where P_K subjected to equ. (11), where a set of planes, or a set of discrete points and kernels, for the union of multiple sphere cores is belonging to the approximation plane.

2.2.1.2 The definition of emotion cell element

The shell of the meta-KANSEI model reflects the range of the model, which is a boundary of uncertainty. However, it is uncertain due to the soft membrane. An approximate boundary for the definition of a shell associated with a given conspiracy parameter is defined as follows:

Definition 7: Define the upper approximation shell of the variable domain (Upper Shell) is $UP_B = \{P_l \mid P_l \in N_{P_K}^{\varepsilon_u}\}$ and the lower approximation shell of the variable domain (Lower Shell) is $LP_B = \{P_l \mid P_l \in N_{P_K}^{\varepsilon_l}\}$. Then, the cell shell is variable neighborhood band, which is given by $P_B = UP_B \setminus LP_B$ noted as $g(x, y)$, parameters x, y are related with density function which will be acquired from the density function, and P_K is the corresponding single-point set, sphere set and plane set of the kernel.

2.2.2 Kernel density estimation segmenting for fMRI dataset

The proposed modeling method and definitions in Section 2.2.1.1 shows that the model is a probability model, and KDE also is calculated using probability. The computing method is introduced by Defs. 4-6 A simple kernel density estimate produces an estimate of the probability distribution function $f(x)$ of the load x using past observations $\{x_i\}$ is given by:

$$\hat{f}_h(x) = \frac{1}{nh}\sum_{i=1}^{n} K(\frac{x - x_i}{h}) \tag{12}$$

where $k(\cdot)$ is the kernel and $h > 0$ is a bandwidth (i.e. smooth parameter) Several types of kernel functions are commonly used, including uniform, triangular, cosine, triweight, Epanechnikov, and Gaussian as follows:

(1) Uniform: $K(u) = \frac{1}{2}$

(2) Triangular: $K(u) = (1 - |u|)$

(3) Cosine: $K(u) = \mathrm{Cos}(u)$

(4) Epanechnikov: $K(u) = \frac{3}{4}(1-u^2)$

(5) Triweight: $K(u) = \frac{35}{32}(1-u^2)^3$

(6) Gaussian: $K(u) = \frac{1}{\sqrt{2\pi}} e^{-\frac{1}{2}u^2}$

Fig.4 illustrates the kernel histogram as examples for KDE (bandwidth distribution approximated is Gaussian distribution).

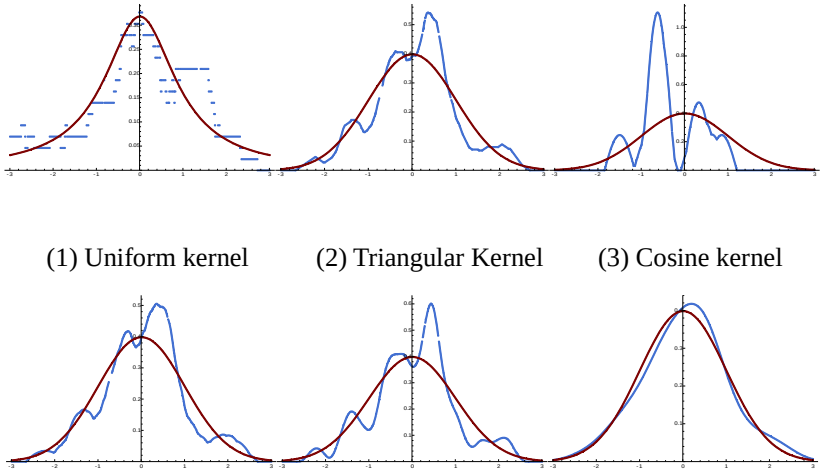

(1) Uniform kernel (2) Triangular Kernel (3) Cosine kernel

(4) Epanechnikov Kernel (5) Trweight Kernel (6) Gaussian kernel

Figure 4. Typical KDE kernels

In the current work, the Gaussian kernel was adopted for bandwidth, where the basic KDE algorithm is as reported in Algorithm 1 [62].

Algorithm 1: Basic Kernel Density Estimation

Start

Input the dataset $X = \{x_1, x_2, ..., x_n\}$

Find m grid points subjected that to $y_i = x_{\min} + i\frac{(x_{\max} - x_{\min})}{m}$, $i = 1, 2, ..., m$

Compute the bandwidth for KDE as $Min\{\sigma, \frac{IQR}{c}\}n^{-b}$

Calculate the KDE using Eqn. (12)

Find the first local minimum point of KDE as y_j^*

If pixel $x_i > y_j^*$

then set the pixel in foreground
Else set the pixel as background
Endif
End

Where, σ is the standard deviation of X, IQR (interquartile range), which is the measure of statistical dispersion and equals to the difference between the upper and lower quartiles, and b is a given constant. Therefore, the proposed Gaussian based KDE algorithm in the current work is given in Algorithm 2.

Algorithm 2: Proposed Gaussian based KDE algorithm

Start

Set the initial values as $k = 0$

Set the foreground of fMRI's mean and standard deviation be μ_f and σ_f and background of fMRI's mean and standard deviation be μ_b and σ_b , μ_f *and* μ_b *are set to the first and third quartiles of pixel intensities in one spot. Initial* σ_f *and* σ_b *are the standard deviations of the pixel intensities below the first quartile and above the third quartile, respectively. Initial* π_1 *and* π_2 *values are set to 0.5.*

Define $f_m(x_i, \mu_m, \sigma_m^2) = \dfrac{1}{\sqrt{2\pi\sigma_m^2}} e^{-\frac{(x_i-\mu_m)^2}{2\sigma_m^2}}$

Calculate $\varphi_{im}^{(k)} = \dfrac{\pi_m^{(k)} f_m(x_i, \mu_m^{(k)}, \sigma_m^{2(k)})}{\pi_1^{(k)} f_1(x_i, \mu_1^{(k)}, \sigma_1^{2(k)}) + \pi_2^{(k)} f_2(x_i, \mu_2^{(k)}, \sigma_2^{2(k)})}$

Calculate new estimates using:

$$\psi^{(k+1)} = \{\pi_m^{(k+1)}, \mu_m^{(k+1)}, \sigma_m^{2(k+1)}, m = 1, 2, \ldots\}$$

$$= \{\frac{1}{n}\sum_{i=1}^{n} \varphi_{im}^{(k)}, \frac{\sum_{i=1}^{n} \varphi_{im}^{(k)} x_i}{\sum_{i=1}^{n} \varphi_{im}^{(k)}}, \frac{\sum_{i=1}^{n} \varphi_{im}^{(k)} (x_i - \mu_m^{(k+1)})^2}{\sum_{i=1}^{n} \varphi_{im}^{(k)}}, m = 1, 2, \ldots\}$$

If $\log(L(\psi^{(k+1)}) - \log L(\psi^{(k)}) < t$ (a given tolerance) then end

Else $k = k+1, \psi^{(k)} = \psi^{(k+1)}$ **Goto** calculating $\varphi_{im}^{(k)}$

Endif

Calculate $\varphi_{im}^{(k+1)} = \dfrac{\pi_m^{(k+1)} f_m(x_i, \mu_m^{(k+1)}, \sigma_m^{2(k+1)})}{\pi_1^{(k+1)} f_1(x_i, \mu_1^{(k+1)}, \sigma_1^{2(k+1)}) + \pi_2^{(k+1)} f_2(x_i, \mu_2^{(k+1)}, \sigma_2^{2(k+1)})}$

Segment the pixel x_i into foreground or background based on $\varphi_{im}^{(k+1)}$ (it is the maximum of posterior probabilities of final values)

End

Where, μ_f and μ_b as the first and third quartiles of pixel intensities, σ_f be the standard deviation of pixel intensities below the first quartile and σ_b be above the third quartile of the same. $\pi_1 = \pi_2 = \dfrac{1}{2}$

The main goal of the work is to segment the fMRI images. Then, sub images will undergo clustering to find their central points and be compared with ANEW experiments. Consequently, to validate the meta-KANSEI modeling methods, the clustering algorithm was introduced in Section 3.2.3.

2.2.3 Mean shift clustering for fMRI dataset

Introduce the Gaussian mean shift and given n sample points in d -dimensional Eula space- $\mathbb{R}$ as $\{x_i, i = 1, 2, ..., n\}$. The kernel density estimation formula is expressed using the Gaussian kernel function $K_N(x) = \dfrac{1}{\sqrt{(2\pi)^d}} e^{-\|x\|^2}$ and the positive definite $d \times d$ bandwidth matrix H_i as:

$$\hat{f}(x) = \frac{1}{\sqrt[d]{2\pi}} \sum_{i=1}^{n} w_i \frac{1}{\sqrt{|H_i|}} e^{\frac{1}{\sqrt{\|x - x_i\|_{H_i}}}} \tag{13}$$

where w_i represents the weights of sample points $\{x_i, i = 1, 2, ..., n\}$ subjected to $\sum_{i=1}^{n} w_i = 1$, and $(x - x_i) H_i (x - x_i)$ indicates the covariance distance of the data. It is an effective method to calculate the similarity of two unknown sample sets, where $\hat{f}(x)$ is the sum of the weighted Gaussian kernel at each point. The estimation on density gradient is given by:

$$\begin{aligned} \nabla \hat{f}(x) &= \frac{1}{\sqrt[d]{2\pi}} \sum_{i=1}^{n} w_i \frac{1}{\sqrt{|H_i|}} \frac{1}{H_i} (x - x_i) e^{-\frac{1}{2}\|x - x_i\|_{H_i}^2} \\ &= \hat{f}(x) \sum_{i=1}^{n} \frac{1}{H_i} (x - x_i) \end{aligned} \tag{14}$$

where H_x is given by:

$$H_x = \frac{\sum_{i=1}^{n} \frac{1}{\sqrt{|H_i|}} e^{-\frac{1}{2}\|x-x_i\|^2_{H_i}}}{\sum_{i=1}^{n} \frac{1}{\sqrt{|H_i|}} \frac{1}{H_i} e^{-\frac{1}{2}\|x-x_i\|^2_{H_i}}} \tag{15}$$

Replace $\nabla \hat{f}(x)$:

$$H_x \nabla \hat{f}(x) = \hat{f}(x)(H_x \frac{\nabla \hat{f}(x)}{\hat{f}(x)}) \tag{16}$$

Thus, $\left(H_x \frac{\nabla \hat{f}(x)}{\hat{f}(x)} + x \right)$ is known as the mean shift vector denoted as $m(x)$, given by:

$$m(x) = \frac{\sum_{i=1}^{n} w_i \frac{1}{\sqrt{|H_i|}} \frac{1}{H_i} e^{-\frac{1}{2}\|x-x_i\|^2_{H_i}} x_i}{\sum_{i=1}^{n} w_i e^{-\frac{1}{2}\|x-x_i\|^2_{H_i}}} \tag{17}$$

From equation (17), let $H = h^2 I$, thus:

$$m(x) = \frac{\sum_{i=1}^{n} w_i e^{-\frac{1}{2}\|\frac{x-x_i}{h}\|^2} x_i}{\sum_{i=1}^{n} w_i e^{-\frac{1}{2}\|\frac{x-x_i}{h}\|^2}} \tag{18}$$

Define $M(x) = m(x) - x$, thus the definition of the kernels type is:

$$K(x) = k \| x \|^2 \tag{19}$$

where k is non-negative, non-increasing and piecewise continuous and $\int_0^\infty k(r)dr < \infty$, where flat kernel is $k(x) = \begin{cases} 1 & x \le \lambda \\ 0 & x > \lambda \end{cases}$ and $k(x) = e^{\frac{\|x\|^2}{2\sigma^2}}$ with standard deviation parameter σ as the bandwidth parameter. Typically, the mean shift is a hill climbing algorithm shifting the kernel iteratively to higher density region. In addition, the mean shift vector will be toward the maximum direction of density. For image clustering, the pseudo-code of the mean shift algorithm is used as presented in Algorithm 3:

Algorithm 3: MEAN_SHIFT (ser, p)

Input: p-*X POINTS, ser*

Output: *pre_w*

[m n]←size(ser)

Tmp←double(ser)

pre_w←tmp(p)

point←p

While 1

ser=tmp-pre_w;

For i←1 to m*n

If *i <> point*

ser(i)←ser(i)/(i-point)

Endif

Endfor

ser←ser.^2

//GAUSSIAN KERNEL

K←(1/sqrt (2*pi)) * exp(-0.5*ser)

W←sum (tmp. * (K))/sum(K)

//GIVEN A THRESHOLD 0.01

If abs(w-pre_w) < 0.01

Goto End

Endif

pre_w←w;

End While

End

Afterwards, the k -mean algorithm is used in the present work, which has been widely used in clustering in order to validate our model by employing the combined dataset from the fMRI calculation and the IAPS experiment. The k-mean algorithm goal is to find the centers of the group that have a significant role in the comparison process during the current work. The proposed algorithm works by dividing n samples into k groups, and randomly selecting one element in each group as the cluster center. Then, the distance from other sampling points to the center is obtained. The sampling points are classified into the class with the smallest Euclidean distance. The average of the sampling points in the newly formed cluster is calculated and a new cluster center is obtained. This procedure is repeated until each sample is categorized correctly. Generally, the *k*-means clustering algorithm is a non-parameter classification method, which is more suitable for the unknown/non-normal distribution data for image segmentation. The algorithm performs the clustering more accurate when handling these data. At the same time, the *k*-means clustering algorithm principle is simple and easy to understand. It can be easily realized efficiently. The pseudo-code of K-mean is presented in Algorithm 4,

Algorithm 4: *K*-MEANS ALGORITHM

INPUT the data objects N

SELECT arbitrarily k objects as the initial cluster center

CALCULATE the mean value of each cluster (center object)

CALCULATE the distance between each object and the center object

DIVIDE the corresponding object per the minimum distance
RE-CALCULATE the mean (center object) of each cluster
CALCULATE the standard measure function
IF the function converges
TERMINATES the algorithm
ELSE
RETURN TO the mean value calculation step
ENDIF
END

In practice, the image object is not strictly distinguished from the category attribute. Therefore, membership was used to determine the membership of each target sample for better partitioning. The FCM clustering algorithm works by dividing n samples into c groups, obtaining the clustering center of each group, which finally minimizes the objective function of the non-similarity index. The algorithm assigns the membership degree between 0 and 1 to each sample point and judges the degree to which the samples belong to each classification by the membership value. At the same time, there is a membership of the provisions of a sample plus one value. The FCM clustering algorithm gives the membership degree of this method to determine the target sample attribution, making the target classification more reasonable. However, the choice of the initial value is very important for the algorithm. If the selected initial value is too far from the global cluster center then the iteration convergence rate will decrease and the number of iterations may increase, which will increase the computation time. At the same time, per the algorithm principle, the algorithm must be set before several clusters to allow the algorithm to continue. However, in practice, determining several classes is very difficult. Therefore, for FCM clustering, the choice of initial values and the number of classes determine how to make the global optimization of clustering become the key problem of clustering.

The FCM's objective is to find a finite set of $X = \{x_1, x_2, ...x_n\}$ into *c*-fuzzy clusters under selected criterion. The outputs is *c* cluster centers as $\{c_1, c_2, ...c_c\}$, where m is any real number greater than 1, and ε is a termination criterion between 0 and 1. The pseudo-code of FCM is given in Algorithm 5.

Algorithm 5: FUZZY C-MEANS ALGORITHM

***Input*:** $X = \{x_1, x_2, ...x_n\}$, cluster numbers: c

Output*:** $\{c_1, c_2, ...c_c\}$ ***and w_{ij}

***Initialize*:** $W = \{w_{ij}\}$ *matrix* $W^{(0)}$

At k ***-Step*****:** *calculate the centers vectors* $C^{(k)} = \{c_j\}$ *with* $W^{(k)}$

$$c_j = \frac{\sum_{i=1}^{n} w_{ij}^m \cdot x_i}{\sum_{i=1}^{n} w_{ij}^m}$$

Update $W^{(k)}$ *and* $W^{(k+1)}$ by

$$w_{ij} = \frac{1}{\sum_{k=1}^{c} \left(\frac{\| x_i - c_j \|}{\| x_i - c_k \|}\right)^{\frac{2}{m-1}}}$$

If $\| W^{(k+1)} - W(k) \| < \varepsilon$ ***Then***

Goto End
Else
Return to *calculating the centers vectors*
Endif
End

3. Results and discussion

3.1 fMRI data acquisition and processing

In the current work, the aim was to obtain brain imaging data under KANSEI stimulation for the case of brain imaging studies of inductive information alone. For this experiment, it was necessary to determine the source of the sensory information (the standard stimulus media), the population to be tested, and the course of the operation. In the selection of standard stimulus media, the IAPS picture library was used. The gallery has been confirmed to have semantically highly correlated properties. In the current study, the IAPS subjective evaluation test program selected and edited 1000 picture data set as the stimulus source. The data set includes several attributes as emotion classification, style description, and subjective evaluation of Valence-Arousal scores and other contextual semantic information. The subjects were mainly college students, screening the basic criteria for the visual normal, no narrow space phobia and other personnel, the subjects were 50 people. The brain imaging equipment was GE Signa HDe1.5T.

The basic process of the experiment was to fix the head of the subject with a fixed band to reduce the movement of the head. The subject receives sensory information stimulation (projection mirror replays mode). The fast spin echo (FSE) is used to acquire the anatomical image. For each group of five subjects, the same set of pictures was taken and the brain imaging data of the subjects were recorded simultaneously. Each participant completed 20 images of the brain imaging test, the total test duration of each subject was approximately 10 minutes, and the complete test period was 6 months.

The brain imaging analysis process was divided into three stages, namely: alignment overlay, brain data extraction, data de-noising and dimension reduction and feature extraction. First, the alignment of superposition, where each image corresponding to the five brain imaging data sets is aligned superimposed to obtain the corresponding image of each brain image volume data set. The brain area data extraction is the location of the brain region that is responsible for emotional Valence response, emotional Arousal response area; respectively, extract the corresponding volume data. The obtained volume data is still high-dimensional image data, and meaningful sensibility indexes needed to be processed by de-noising and dimension reduction. After the data normalization processing, the expected dimension of the brain imaging data was still highly-dimensional and need a variety of dimensionality reduction methods to be applied, such as linear dimension reduction, down-sampling, preservation structure dimension reduction methods; respectively. After these steps, a regular brain imaging data set is obtained. Table 1 reported the device parameters as well as the values in the fMRI experiment.

Table 1. The parameters and the values of dataset in the fMRI experiment

Parameters	**Value**	**Parameters**	**Value**
Acquisition Time	105516.443844	GE medical systems	Manufacturer
SLICE Thickness	6.0000	Echo Time	113.792
Echo Train Length	28	Imaging Frequency	63.873271
Magnetic Field Strength	1.50000	Spacing Between Slice	6.80000
Flip Angle	90.0	Patient Position	HFS

The original fMRI data by GE Signa HDe1.5T., from KANSEI stimuli experiment is listed in Fig.5.

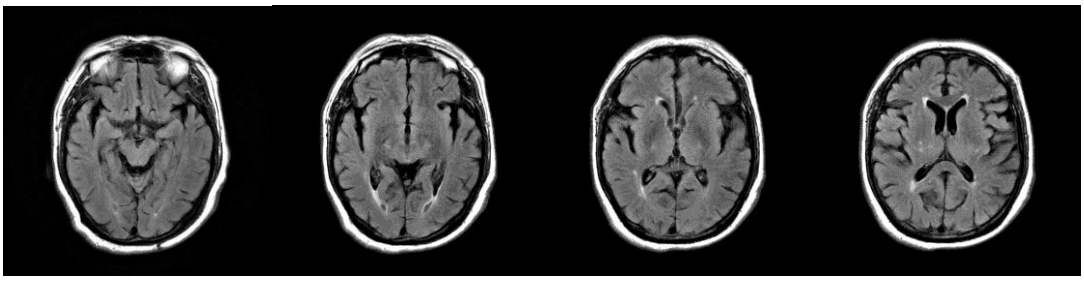

Figure 5. The typical fMRI data from KANSEI stimuli experiments

The KDE segmentation is acquired using smoothed with kernel density estimation images as illustrated in Fig. 5. The fMRI dataset segmentation with Gaussian based kernel density estimation is shown in Fig.6.

Figure 6. fMRI dataset segmentation with Gaussian based kernel density estimation

As segmentation with Gaussian based KDE operating, the ROI was separated from the dataset. Thus, the zone of mygdala and orbitofrontal cortex is located, which is relative to the Valence-Arousal as shown in Fig.7.

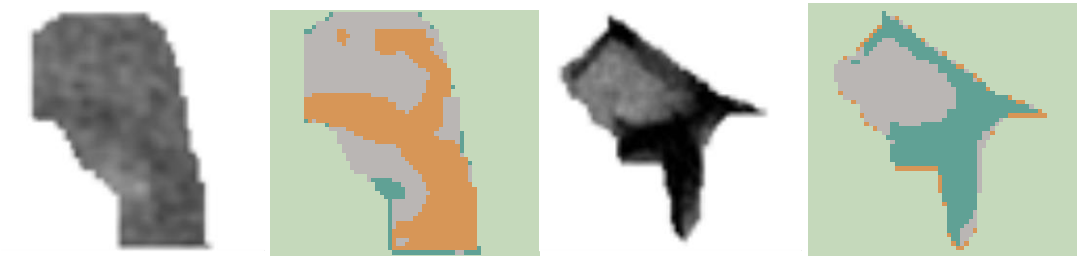

(1) (2) (3) (4)

Figure 7. The region of interest of fMRI dataset relative to Valence as (1) mygdala (2) clustering on mygdala and Arousal as (3) orbitofrontal cortex (4) clustering on orbitofrontal cortex

To obtain 20 images from the brain imaging test, 20 Valence related fMRI images and 20 Arousal related fMRI images were acquired. Afterwards, the fuzzy c-means algorithm was applied to find the cluster center of each related fMRI dataset of Valence-Arousal zone under 4 KANSEI adjectives being angry, happy, sad, pleasant, so that we could compare the results with the IAPS experiment in Section 4.2. to show the feasibility of the modeling method proposed work. The data of the FCM operating with fMRI dataset was listed in Section 4.3.

3.2 ANEW systems by IAPS experiments

For comparative study, the experiment was performed on an emotional set of pictures, that is, the subjects were asked to complete the same 20 pictures Valence-Arousal labeling. In addition, 50 subjects were still labeled with the same picture set by averaging or median method to get Valence-Arousal value of each picture.

ANEW, created by Bradley and Cuthbert, is a set of normative emotional ratings for many words in the English language under the IAPS (International Affective Picture System) project [9]. The KANSEI adjectives were coordinated by Valence-Arousal as shown in Appendix I: ANEW system.

The obtained results in Appendix I. established that a total of 1033 KANSEI adjectives were valued by Valence-Arousal through the Self-Assessment Manikin (SAM) experimental method by Bradley and Cuthbert; and Valence_SD and Arousal_SD present the standard deviation of Valence and Arousal.

The ANEW system assumes that emotions can be measured using a dimensional scale based on Osgood's semantic differential theory (SDT). The basic method for processing those values relatives to a certain semantic was clustered in the previous study; normally scatter plot is illustrated in Fig. 8 and then defined the distance between the semantics for clustering. Appendix II reported 80 pairs from the IAPS experiment with the Valence-Arousal calculations.

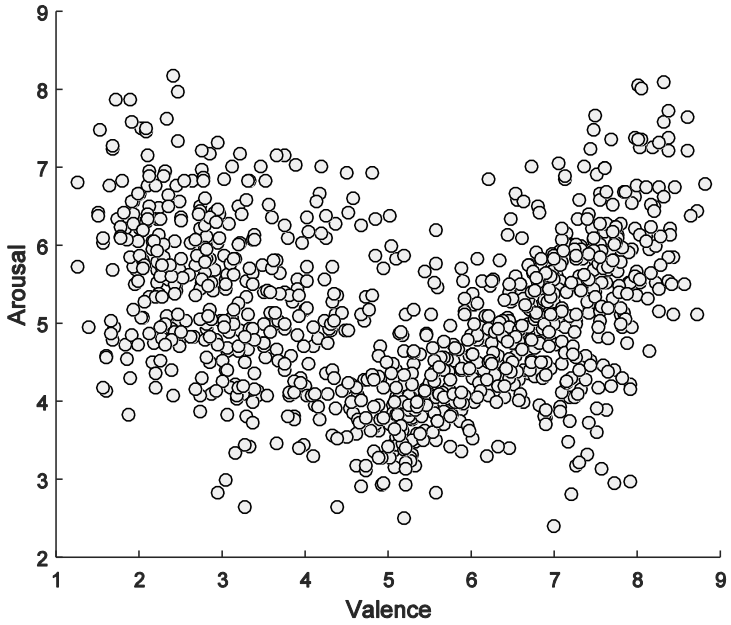

Figure 8. 1033 semantic words in Valence-Arousal space

All Valence -Arousal experiments followed the ANEW method and are listed in Appendix II. It established that 80 pair values of Valence-Arousal for the 4 KANSEI adjectives of angry, happy, sad and pleasant. Afterwards, the fuzzy *c*-means was started with 2 exponent and maximum 100 iterations, achieving minimum improvement of 10^{-5}. The cluster number is 4 and relative to the 4 adjectives of angry, happy, sad, and pleasant. Figure 9 demonstrates the 4 clusters of fuzzy *c*-means algorithm using combined dataset from IAPS experiment.

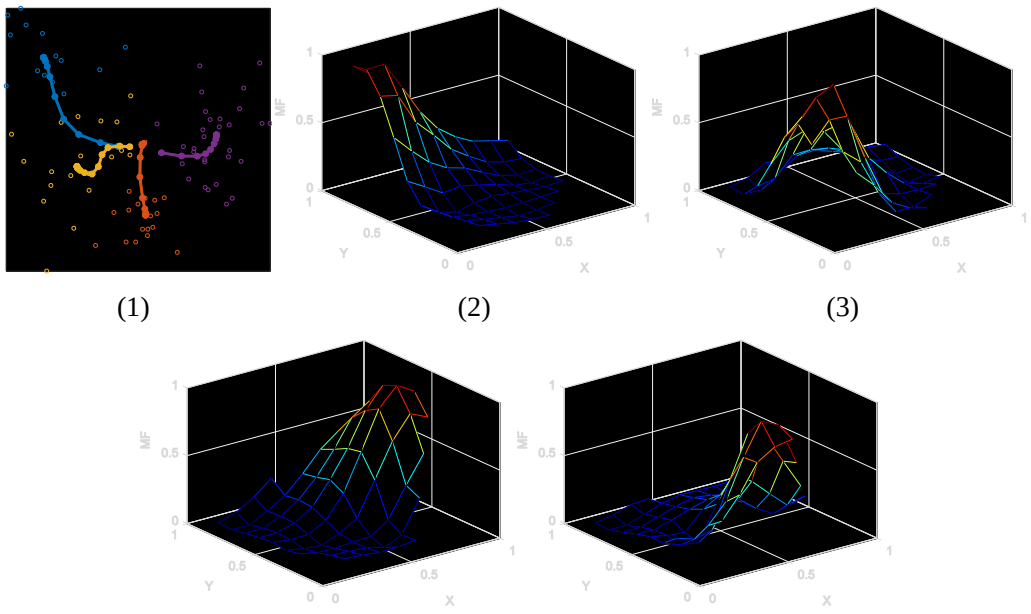

Figure 9. 4 clusters of fuzzy *c*-means algorithm using combined dataset from IAPS experiment and

calculation of Valence-Arousal related fMRI images and (1) is clustering, (2) -(5) are membership function of each clusters.

The iteration values were visualized in Fig. 10, after 30 iterations, the objective function of the FCM is stable referring to the given threshold ε.

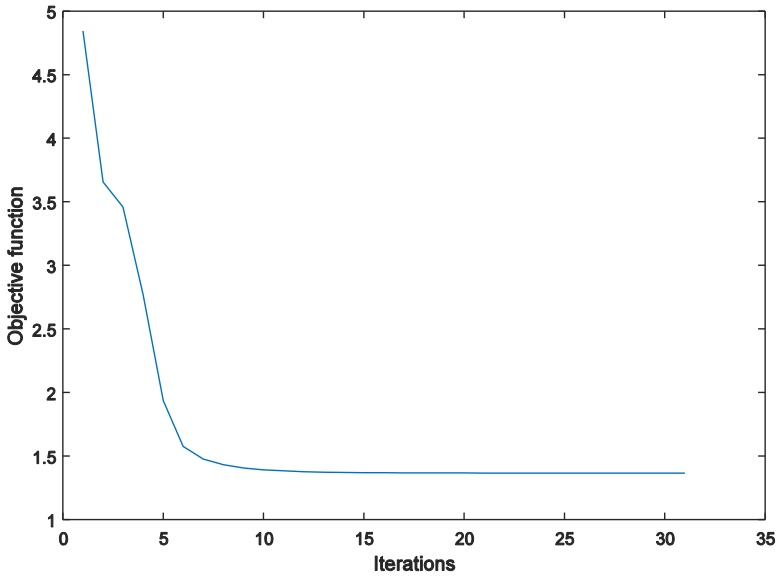

Figure 10. The iterations of objective function by FCM with the combined dataset.

Figure 10 establishes that the objective function, which denotes the distance between the pixels and center of each clusters, is minimized with the increased number of iterations. As from Fig. 10, we know that the objective function is stable and kept within 1.5 after 10 iterations.

3.3 Comparing with ANEW system and fMRI dataset

20 brain images with KDE segmentation and mean shift clustering were compared with ANEW under the IPAS experiment. Thus, data two parts were listed in Table 2 and all values were also normalized. To validate the feasible of meta-KANSEI modeling method proposed in the current work, the distance of these two datasets was calculated. Since the meta-KANSEI model is a cellular based model with kernel center and radius for the shell, the distance of these two datasets is definite under the 4 adjectives (angry, happy, sad, and pleasant) of Valence-Arousal with radius (the fuzzy membership w_{ij} by FCM calculation in Section 4.2). Similarity computing was introduced in previous studies [64-67]. The distance is redefined using the following expression:

$$d = \sqrt{(x_f r_f - x_a r_a)^2 + (y_f r_f - y_a r_a)^2} \tag{20}$$

where, x_f, y_f is center of fMRI dataset, r_f is radius of cluster of fMRI dataset while x_a, y_a, r_a are for ANEW dataset.

Table 2. The dataset of fMRI and ANEW under FCM operating

fMRI						ANEW					
Center		r	Center		r	Center		r	Center		r
0.83	0.60	0.24	0.44	0.48	0.34	0.44	0.48	0.48	0.37	0.67	0.67
0.39	0.64	0.23	0.81	0.61	0.28	0.81	0.61	0.61	0.81	0.46	0.46
0.91	0.81	0.25	0.34	0.52	0.59	0.34	0.52	0.52	0.62	0.43	0.43
0.68	0.46	0.31	0.50	0.55	0.48	0.50	0.55	0.55	0.74	0.48	0.48
0.82	0.51	0.28	0.27	0.54	0.47	0.27	0.54	0.54	0.89	0.61	0.61
0.39	0.52	0.22	0.54	0.48	0.68	0.54	0.48	0.48	0.47	0.62	0.62
0.69	0.48	0.30	0.78	0.62	0.49	0.78	0.62	0.62	0.84	0.69	0.69
0.78	0.59	0.34	0.27	0.81	0.39	0.27	0.81	0.81	0.55	0.55	0.55
0.40	0.63	0.30	0.84	0.54	0.42	0.84	0.54	0.54	0.40	0.40	0.40
0.19	0.53	0.27	0.26	0.85	0.43	0.26	0.85	0.85	0.47	0.72	0.72
0.37	0.44	0.17	0.32	0.80	0.53	0.32	0.80	0.80	0.80	0.55	0.55
0.82	0.59	0.27	0.24	0.59	0.40	0.24	0.59	0.59	0.58	0.40	0.40
0.35	0.56	0.33	0.59	0.46	0.52	0.59	0.46	0.46	0.35	0.75	0.75
0.28	0.73	0.28	0.30	0.72	0.38	0.30	0.72	0.72	0.74	0.54	0.54
0.29	0.67	0.26	0.74	0.60	0.71	0.74	0.60	0.60	0.51	0.62	0.62
0.39	0.78	0.27	0.53	0.77	0.39	0.53	0.77	0.77	0.67	0.35	0.35
0.71	0.56	0.32	0.83	0.64	0.45	0.83	0.64	0.64	0.37	0.74	0.74
0.46	0.44	0.30	0.57	0.45	0.37	0.57	0.45	0.45	0.44	0.51	0.51
0.54	0.41	0.14	0.59	0.40	0.77	0.59	0.40	0.40	0.55	0.67	0.67
0.58	0.36	0.33	0.52	0.56	0.60	0.52	0.56	0.56	0.46	0.37	0.37
0.70	0.51	0.35	0.89	0.74	0.31	0.89	0.74	0.74	0.54	0.44	0.44
0.54	0.51	0.22	0.41	0.63	0.60	0.41	0.63	0.63	0.42	0.55	0.55
0.66	0.49	0.28	0.74	0.54	0.36	0.74	0.54	0.54	0.80	0.45	0.45
0.37	0.42	0.20	0.34	0.70	0.50	0.34	0.70	0.70	0.34	0.49	0.49
0.88	0.66	0.16	0.23	0.83	0.79	0.23	0.83	0.83	0.77	0.49	0.49
0.45	0.45	0.27	0.73	0.73	0.63	0.73	0.73	0.73	0.32	0.46	0.46
0.91	0.72	0.16	0.74	0.59	1.06	0.74	0.59	0.59	0.71	0.56	0.56
0.58	0.57	0.30	0.73	0.68	0.46	0.73	0.68	0.68	0.32	0.71	0.71
0.27	0.53	0.29	0.71	0.50	0.49	0.70	0.50	0.50	0.81	0.56	0.56
0.61	0.46	0.75	0.37	0.62	0.93	0.37	0.62	0.62	0.39	0.51	0.51
0.81	0.66	0.27	0.61	0.46	0.65	0.61	0.46	0.46	0.75	0.48	0.48
0.38	0.46	0.29	0.74	0.64	0.41	0.74	0.64	0.64	0.54	0.37	0.37
0.39	0.55	0.25	0.91	0.61	0.52	0.91	0.61	0.61	0.62	0.61	0.61
0.35	0.45	0.33	0.69	0.57	0.56	0.69	0.57	0.57	0.76	0.62	0.62
0.31	0.51	0.25	0.50	0.43	0.61	0.50	0.43	0.43	0.23	0.79	0.79
0.81	0.60	0.24	0.22	0.69	0.15	0.22	0.69	0.69	0.64	0.46	0.46
0.85	0.63	0.31	0.60	0.43	0.13	0.60	0.43	0.43	0.33	0.31	0.31
0.78	0.63	0.25	0.71	0.56	0.29	0.71	0.56	0.56	0.68	0.53	0.53
0.82	0.70	0.25	0.56	0.37	0.22	0.56	0.37	0.37	0.78	0.61	0.61
0.81	0.62	0.29	0.61	0.40	0.81	0.61	0.40	0.40	0.59	0.39	0.39

The results reported in Table 2 establish that 80 pairs $\left(x_f, y_f, r_f\right)$ on the left of the table comes from fMRI dataset while the other 80 pairs $\left(x_a, y_a, r_a\right)$ from ANEWS. To separate the four KANSEI adjectives and compared the difference between two datasets, the normal probability for the 80 distances in 4 groups is plotted in Fig. 11.

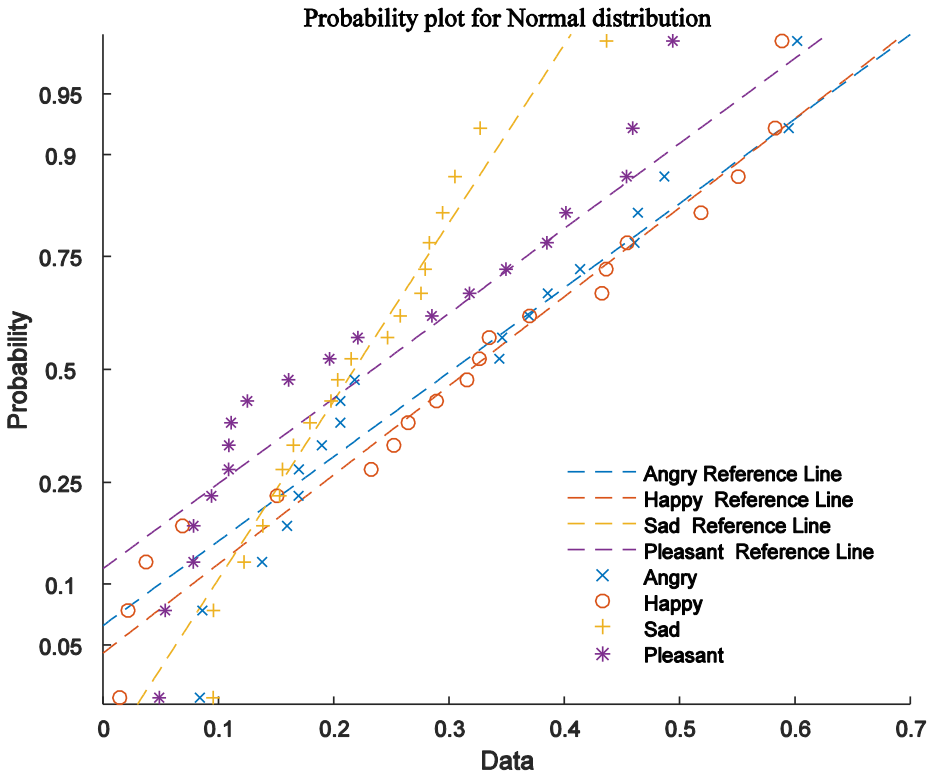

Figure 11. Normal probability for the 80 distances in 4 groups based on the similarity computing on distance between two datasets

Figure 11 shows the feasibility of the proposed modeling method where all adjectives are stable. From the process of the dataset, and for feature extraction of fMRI dataset, the results illustrate that meta-KANSEI modeling using KDE segmentation and mean shift clustering shows a close performance fit with the IAPS experiment dataset by using probability plot. The result provides all the necessary information to reflect the difference between the IAPS system and the proposed methods for fMRI experimental dataset. The proposed modeling method is thus feasible evidenced by the IAPS experiments. Consequently, the proposed system has been established as effective, thus this novel method that applied in the medical imaging dataset can be used for future research as follows: i) the de-dimensionality operation of fMRI dataset needs to be considered using other algorithms such as structure preserve projection, or to be combined with local preserving for fMRI dataset reduction for potential improvement; ii) calculate more features from the fMRI dataset and compare those features in the experiment, iii) more slices need to be extracted for calculating to promote the result in future research, and iv) various datasets that used previously in medical studies can be used to test the proposed system.

4. Conclusion

In this study, a meta-KANSEI modeling method was introduced. In addition, the fMRI experimental dataset was acquired and processed using kernel density estimation-based segmentation and mean shift clustering. The distance between two datasets was calculated for comparison with ANEW dataset under fuzzy *c*-means, and under normal distribution view for typical KANSEI adjectives. The results showed the model feasibility and the performed effectiveness for the experimental methods. By comparing with our previous studies [44-46], it can be concluded that:

- An innovative processing method for using kernel density segmentation has been presented,
- The mean shift can be used to cluster the acquired segments to remove dimensionality in the dataset,
- An innovative modeling method using central points based meta-KANSEI model combined the advantages of a variety of existing intelligent processing methods has been presented.

Compliance with Ethical Standards:
Funding: This study was funded by Zhejiang Provincial Natural Science Foundation (LY17F030014)
Ethical approval: All procedures performed in studies involving human participants were in accordance with the ethical standards of the institutional and/or national research committee and with the 1964 Helsinki declaration and its later amendments or comparable ethical standards.
Informed consent: Informed consent was obtained from all individual participants included in the study.

References

[1] Muhammad Y, Zhang D. Anatomical pattern analysis for decoding visual stimuli in human brains, Cognitive Computation, 2018; 10(2): 284–295
[2] Wang S, Fu B, Zhao W, Liu Y, Wei F. Structure, function, and dynamic mechanisms of coupled human–natural systems, Current Opinion in Environmental Sustainability, 2018; 33, 87-91
[3] Guerar M, Merlo A, Migliardi M. Completely Automated Public Physical test to tell Computers and Humans Apart: A usability study on mobile devices, Future Generation Computer Systems, 2018; 82, 617-630
[4] Poria S, Cambria E, Bajpai R, Hussain A; A review of affective computing: From unimodal analysis to multimodal fusion, Information Fusion, 2017; 37, 98-125
[5] Lang PJ, Bradley MM, Cuthbert BN. International affective picture system (IAPS): Affective ratings of pictures and instruction manual. Technical Report A-8, University of Florida, Gainesville, FL, 2008
[6] Mehrabian A. An approach to environmental psychology, Cambridge, MA: MIT Press, 1974
[7] Bellezza FS, Greenwald AG, Banaji MR. Words high and low in pleasantness as rated by male and female college students, Behavior Research Methods, Instruments & Computers, 1986; 18 (3): 299-303
[8] Bradley MM, Lang PJ. Affective norms for English words (ANEW): Instruction manual and affective ratings. Technical Report C-1, The Center for Research in Psychophysiology, University of Florida, 1999

[9] Nagamachi M. KANSEI engineering: a new ergonomics consumer-oriented technology for product development, International Journal of Industry Design, 1995; 15 (1): 3-11

[10] Yeh CT, Chen MC. Applying Kansei engineering and data mining to design door-to-door delivery service, Computers & Industrial Engineering, 2018; 120, 401-417

[11] Shieh MD, Li Y, Yang CC. Comparison of multi-objective evolutionary algorithms in hybrid Kansei engineering system for product form design, Advanced Engineering Informatics, 2018 36, 31-42

[12] Takenouchi H, Tokumaru M. Kansei retrieval agent model with fuzzy reasoning, International Journal of Fuzzy Systems, 2017; 19(6): 1803–1811

[13] Wang D, Li Z, Dey N, Ashour AS, Sherratt RS, Shi F. Case-based reasoning for product style construction and fuzzy analytic hierarchy process evaluation modeling using consumers linguistic Variables, IEEE Access, 2017; 5: 4900-4912

[14] Cao L, Li J, Xu Y, Zhu H, Jiang C. A hybrid vigilance monitoring study for mental fatigue and its neural activities, Cognitive Computation, 2016; 8(2): 228–236

[15] Li J, Zhang Z, He H. Hierarchical convolutional neural networks for EEG-based emotion recognition, Cognitive Computation, 2018; 10(2):368–380

[16] Burgués J, Jiménez-Soto JM, Marco S. Estimation of the limit of detection in semiconductor gas sensors through linearized calibration models, Analytica Chimica Acta, 2018; 1013, 13-25

[17] Mayhew SD, Mullinger KJ, Ostwald D, Porcaro C, Bowtell R, Bagshaw AP, Francis ST. Global signal modulation of single-trial fMRI response variability: effect on positive vs negative BOLD response relationship, NeuroImage, 2016; 133, 62-74

[18] Seidel M, King JA, Ritschel F, Boehm I, Geisler D, Bernardoni F, Beck M, Pauligk S, Biemann R, Strobel A, Goschke T, Walter H, Roessner V, Ehrlich S. Processing and regulation of negative emotions in anorexia nervosa: an fMRI study, NeuroImage: Clinical, 2018; 18, 1-8

[19] Xie W, Peng CK, Huang CC, Lin CP, Tsai SJ, Yang AC. Functional brain lateralization in schizophrenia based on the variability of resting-state fMRI signal, Progress in Neuro-Psychopharmacology and Biological Psychiatry, 2018; 86, 114-121

[20] Kensinger E A, Corkin S. Two routes to emotional memory: distinct neural processes for valence and arousal, PNAS, 2004; 101(9):3310-3315

[21] Kensinger EA, Schacter DL. Processing emotional pictures and words: effects of valence and arousal, Cognitive, Affective, & Behavioral Neuroscience, 2006; 6(2):110-116

[22] He T, Cao L, Balas VE, McCauley P, Shi F. Curvature manipulation of the spectrum of valence-arousal-related fMRI dataset using gaussian-shaped fast fourier transform and its application to fuzzy KANSEI adjectives modeling, Neurocomputing, 2016; 174, Part B, 1049-1059

[23] Wu L, Tang Z, Feng X, Sun X, Qian W, Wang J, Jin L, Jiang J, Zhong Y. Metabolic changes in the bilateral visual cortex of the monocular blind macaque: a multi-voxel proton magnetic resonance spectroscopy study, Neurochemical Research, 2017; 42(2): 697–708

[24] Janata P, Birk JL, Van Horn JD, Leman M, Tillmann B, Bharucha JJ. The cortical topography of tonal structures underlying western music, Science, 2002; 298(13):2167-2170

[25] Müller-Bardorff M, Bruchmann M, Mothes-Lasch M, Zwitserlood P, Schlossmacher I, Hofmann D, Miltner W, Straube T. Early brain responses to affective faces: a simultaneous EEG-fMRI study, NeuroImage, 2018; 178, 660-667

[26] Thibault RT, MacPherson A, Lifshitz M, Roth RR, Raz A. Neurofeedback with fMRI: a critical

systematic review, NeuroImage, 2018; 172, 786-807

[27] Cherubini A, Caligiuri ME, Péran P, Sabatini U, Cosentino C, Amato F. Importance of multimodal MRI in characterizing brain tissue and its potential application for individual age prediction, IEEE Journal of Biomedical and Health Informatics, 2016; 20(5):1232 – 1239

[28] Sardouie SH, Shamsollahi MB, Albera L, Merlet I. Denoising of ictal EEG data using semi-blind source separation methods based on time-frequency priors, IEEE Journal of Biomedical and Health Informatics, 2015; 19(3):839 – 847

[29] Frantzidis CA, Bratsas C, Papadelis CL, Konstantinidis E, Pappas C, Bamidis PD. Toward emotion aware computing: an integrated approach using multichannel neurophysiological recordings and affective visual stimuli, IEEE Transactions on Information Technology in Biomedicine, 2010; 14(3):589-597

[30] Murugappan M, Rizon M, Nagarajan R, Yaacob S. Inferring of human emotional states using multichannel EEG, European Journal of Scientific Research, 2010; 48(2): 281-299

[31] Hui T, Sherratt RS. Coverage of emotion recognition for common wearable biosensors, Biosensors 2018, 8, 30, doi: 10.3390/bios8020030

[32] Haben S, Giasemidis G. A hybrid model of kernel density estimation and quantile regression for GEFCom2014 probabilistic load forecasting, International Journal of Forecasting 2016, 32: 1017-1022

[33] Miao S, Xie K, Yang H, Karki R, Tai HM, Chen T. A mixture kernel density model for wind speed probability distribution estimation, Energy Conversion and Management, 2016; 126: 1066-1083

[34] Yuan Y, Wan J, Wang Q. Congested scene classification via efficient unsupervised feature learning and density estimation, Pattern Recognition, 2016; 56: 159-169

[35] Rodrigues GS, Nott DJ, Sisson SA. Functional regression approximate bayesian computation for gaussian process density estimation, Computational Statistics and Data Analysis, 2016; 103: 229-241

[36] Tao Z, Han B, Chen H. On intuitionistic fuzzy copula aggregation operators in multiple-attribute decision making, Cognitive Computation 2018, doi 10.1007/s12559-018-9545-1

[37] Ren P, Sun W, Luo C, Hussain A. Clustering-oriented multiple convolutional neural networks for single image super-resolution, Cognitive Computation, 2018; 10(1): 165–178

[38] Ghassabeh YA. On the convergence of the mean shift algorithm in the one-dimensional space, Pattern Recognition Letters, 2013; 34: 1423-1427

[39] Ibrahim MM, Soraghan JJ, Petropoulakis L. Eye-state analysis using an interdependence and adaptive scale mean shift (iasms) algorithm, Biomedical Signal Processing and Control, 2014; 11:53-62

[40] Duong T, Beck G, Azzag H, Lebbah M. Nearest neighbour estimators of density derivatives, with application to mean shift clustering, Pattern Recognition Letters, 2016; 80: 224-230

[41] Chen W, Li Q, Dahal K. ROI image retrieval based on multiple features of mean shift and expectation-maximisation, Digital Signal Processing, 2015; 40: 117-130

[42] Ai L, Xiong J. Temporal-spatial mean-shift clustering analysis to improve functional MRI activation detection, Magnetic Resonance Imaging, 2016; 34: 1283-1291

[43] Ghassabeh YA, Rudzicz F, The mean shift algorithm and its relation to kernel regression, Information Sciences, 2016; 348: 198-208

[44] Dey N, Ashour AS, Beagum S, Pistola DS, Gospodinov M, Gospodinova EP, Tavares JMRS. Parameter optimization for local polynomial approximation based intersection confidence interval

filter using genetic algorithm: an application for brain MRI image de-noising. Journal of Imaging, 2015; 1: 60-84

[45] Wang D, He T, Li Q, Cao L, Li Z, Dey N, Ashour AS, Balas VE, McCauley P, Xu J, Shi F. Image features based affective retrieval employing improved parameter and structure identification of adaptive neuro fuzzy inference system, Neural Computing and Applications 2016, doi: 10.1007/s00521-016-2512-4

[46] Dey N, Ashour A, Samanta S, Chakraborty S, Sifaki D, Ashour A, Nguyen NG, Le DN. Healthy and unhealthy rat hippocampus cells classification: a neural based automated system for alzheimer disease classification, Journal of Advanced Microscopy Research, 2016; 11: 1-10

Appendix

I. ANEW system- KANSEI adjectives and their Valence-Arousal scores in SAM rating experiments

Index	Adjectives	Valence	Valence_SD	Arousal	Arousal_SD
1	abduction	2.76	-2.06	5.53	-2.43
2	abortion	3.5	-2.3	5.39	-2.8
3	absurd	4.26	-1.82	4.36	-2.2
4	abundance	6.59	-2.01	5.51	-2.63
5	abuse	1.8	-1.23	6.83	-2.7
6	acceptance	7.98	-1.42	5.4	-2.7
7	accident	2.05	-1.19	6.26	-2.87
…	…	…	…	…	…
1028	reverent	5.35	-1.21	4	-1.6
1029	revolt	4.13	-1.78	6.56	-2.34
1030	revolver	4.02	-2.44	5.55	-2.39
1031	reward	7.53	-1.67	4.95	-2.62
1032	riches	7.7	-1.95	6.17	-2.7
1033	ridicule	3.13	-2.24	5.83	-2.73

II. ANEW System-80 pairs from IAPS experiment and calculation of Valence-Arousal

Angry		Happy		Sad		Pleasant	
V	A	V	A	V	A	V	A
0.439	0.478	0.886	0.737	0.373	0.674	0.543	0.438
0.806	0.611	0.410	0.628	0.814	0.462	0.417	0.548
0.341	0.516	0.742	0.540	0.617	0.431	0.799	0.450
0.498	0.546	0.343	0.698	0.743	0.484	0.339	0.488
0.268	0.537	0.226	0.834	0.892	0.614	0.772	0.490
0.544	0.476	0.729	0.731	0.470	0.619	0.320	0.456
0.782	0.623	0.740	0.587	0.844	0.686	0.714	0.563
0.274	0.814	0.734	0.678	0.546	0.550	0.322	0.712
0.837	0.537	0.700	0.501	0.399	0.401	0.807	0.559
0.260	0.848	0.366	0.616	0.467	0.723	0.391	0.508

0.317	0.797	0.611	0.458	0.804	0.546	0.751	0.479
0.236	0.592	0.744	0.638	0.579	0.399	0.536	0.373
0.586	0.462	0.913	0.614	0.352	0.751	0.617	0.613
0.304	0.721	0.686	0.567	0.742	0.536	0.756	0.622
0.737	0.601	0.504	0.433	0.512	0.617	0.233	0.794
0.534	0.769	0.222	0.690	0.670	0.352	0.636	0.463
0.833	0.644	0.600	0.426	0.366	0.742	0.328	0.314
0.567	0.450	0.713	0.556	0.438	0.512	0.683	0.532
0.593	0.399	0.561	0.373	0.548	0.670	0.780	0.607
0.524	0.559	0.606	0.403	0.456	0.366	0.592	0.386

*All data are normalized